Dissociation limit and dissociation dynamic of CF4+: Application of threshold photoelectron-photoion coincidence velocity imaging

Xiaofeng Tang, Xiaoguo Zhou, Manman Wu, Zhi Gao, Shilin Liu et al.

Citation: J. Chem. Phys. **138**, 094306 (2013); doi: 10.1063/1.4792368
View online: http://dx.doi.org/10.1063/1.4792368
View Table of Contents: http://jcp.aip.org/resource/1/JCPSA6/v138/i9
Published by the American Institute of Physics.

Dissociation limit and dissociation dynamic of CF_4^+: Application of threshold photoelectron-photoion coincidence velocity imaging

Xiaofeng Tang,[1,2] Xiaoguo Zhou,[1,a)] Manman Wu,[1] Zhi Gao,[1] Shilin Liu,[1] Fuyi Liu,[2] Xiaobin Shan,[2] and Liusi Sheng[2]
[1]*Hefei National Laboratory for Physical Sciences at the Microscale and Department of Chemical Physics, University of Science and Technology of China, Hefei, Anhui 230026, China*
[2]*National Synchrotron Radiation Laboratory, University of Science and Technology of China, Hefei, Anhui 230029, China*

(Received 7 December 2012; accepted 1 February 2013; published online 1 March 2013)

Dissociation of internal energy selected CF_4^+ ions in an excitation energy range of 15.40–19.60 eV has been investigated using threshold photoelectron-photoion coincidence (TPEPICO) velocity imaging. Only CF_3^+ fragment ions are observed in coincident mass spectra, indicating all the X^2T_1, A^2T_2, and B^2E ionic states of CF_4^+ are fully dissociative. Both kinetic energy released distribution (KERD) and angular distribution in dissociation of CF_4^+ ions have been derived from three-dimensional TPEPICO time-sliced images. A parallel distribution of CF_3^+ fragments along the polarization vector of photon is observed for dissociation of CF_4^+ ions in all the low-lying electronic states. With the aid of F-loss potential energy curves, dissociation mechanisms of CF_4^+ ions in these electronic states have been proposed. CF_4^+ ions in both X^2T_1 and A^2T_2 states directly dissociate to CF_3^+ and F fragments along the repulsive C-F coordinate, while a two-step dissociation mechanism is suggested for B^2E state: $CF_4^+(B^2E)$ ion first converts to the lower A^2T_2 state via internal conversion, then dissociates to CF_3^+ and F fragments along the steep A^2T_2 potential energy surface. In addition, an adiabatic appearance potential of $AP_0(CF_3^+/CF_4)$ has also been established to be 14.71 ± 0.02 eV, which is very consistent with the recent calculated values. © *2013 American Institute of Physics*. [http://dx.doi.org/10.1063/1.4792368]

I. INTRODUCTION

As a benchmark molecule with high symmetry, ionization and dissociation of tetrafluoromethane (CF_4) have attracted extensive investigations for a long history. It is well known that its valence-shell electronic configuration in ground state is $(3a_1)^2(2t_2)^6(4a_1)^2(3t_2)^6(1e)^4(4t_2)^6(1t_1)^6$ with T_d symmetrical structure,[1] and the Jahn-Teller distortion can reduce its symmetry from T_d to C_{3v}. Once removing one $1t_1$, $4t_2$, or 1e electron from the outer orbitals, CF_4^+ ions in various ionic states, e.g., X^2T_1, A^2T_2, and B^2E, are produced, respectively. Both X^2T_1 and A^2T_2 bands were structureless in photoelectron spectroscopy (PES)[1–3] and threshold photoelectron spectroscopy (TPES),[4,5] while a few weak vibrational bands superimposed on a broad continuum background were observed for the B^2E state.[4,5]

In past decades, dissociation of CF_4^+ ions in the low-lying electronic states has been investigated with many experimental methods, e.g., photoionization,[6,7] electron impact ionization,[8–11] ion-molecule reaction,[12,13] ion imaging,[14] velocity imaging photoionization coincidence (VIPCO),[15] photoelectron fluorescence coincidence,[16,17] photoelectron-photoion coincidence (PEPICO),[18–20] and threshold photoelectron-photoion coincidence (TPEPICO).[5,21,22] Only CF_3^+ fragment ions were observed for dissociation of $CF_4^+(X^2T_1, A^2T_2, \text{and } B^2E)$ ions, while no stable CF_4^+ ions were detected in the most of previous experiments, except that Kime *et al.* observed a very small amount of CF_4^+ ions using electron impact ionization[10] and Hagenow *et al.* detected CF_4^+ in dissociative photoionization (DPI) of the dimmer.[23] Therefore, the ground electronic state of CF_4^+ is generally believed unstable, and both the A^2T_2 and B^2E excited states can also dissociate along a fragmentation pathway.

As the ground electronic state of CF_4^+ ions is dissociative in Franck-Condon region, it is very difficult to directly measure the adiabatic appearance potential $AP_0(CF_3^+/CF_4)$. When CF_4 is photoionized in Franck-Condon region, excess energy above the dissociation limit of $CF_3^+ + F$ will be distributed among internal and kinetic energies (KE) of fragments. Thus an upper limit of $AP_0(CF_3^+/CF_4)$ can be obtained by estimating the released KE from analyzing time-of-flight (TOF) profile of fragments. Using PEPICO technique with He I light source, Brehm *et al.*,[18] Simm *et al.*,[19] and Powis[20], respectively measured the released KE in dissociation of $CF_4^+(X^2T_1)$ ions and proposed the upper limits. By measuring the released KE as a function of excitation energy and assuming that the fractional released KE was independent of ionization energy, Chim *et al.* extrapolated the KE to zero and obtained a lower value of 14.45 eV for $AP_0(CF_3^+/CF_4)$.[21] Besides these direct ionization measurements, the $AP_0(CF_3^+/CF_4)$ value was also derived from thermo-chemical data,[24] ion-molecule reactions[12,13]

a)Author to whom correspondence should be addressed. Electronic mail: xzhou@ustc.edu.cn.

TABLE I. Adiabatic appearance potential $AP_0(CF_3^+/CF_4)$ obtained in different experimental measurements and recent quantum chemical calculations.

AP_0 (eV)	Experimental/theoretical method	Light source	Reference
Experimental			
≤15.35	Photoionization efficiency curve	He Hopfield	6
≤14.84 ± 0.05	PEPICO	He I	18
≤14.90 ± 0.1	PEPICO	He I	19
≤14.7 ± 0.3	PEPICO	He I	20
14.45 ± 0.20	TPEPICO	Synchrotron radiation	21
14.67 ± 0.04	Photoionization and thermodynamic	He Hopfield and H_2 continuum	24
14.24 ± 0.07	Ion-molecule reaction	…	12
14.2 ± 0.1	Ion-molecule reaction	…	13
14.71 ± 0.02	TPEPICO velocity imaging	Synchrotron radiation	This work
Theoretical			
∼14.70	CCSD/Dunning's correlation consistent basis sets[a]	…	25, 27
14.699	W1 and CBS-APNO[b]	…	26

[a]The calculated $\Delta H_{0K}(CF_4)$ and $\Delta H_{0K}(CF_3)$ are –927.8 and –464.8 kJ · mol^{-1}, respectively (Ref. 25). The $IP_{ad.}(CF_3)$ is 9.102 or 9.001 eV and thus $AP_0(CF_3^+/CF_4)$ can be calculated as the formula of $AP_0(CF_3^+/CF_4) = \Delta H_{0K}(CF_3) + IP_{ad.}(CF_3) + \Delta H_{0K}(F) - \Delta H_{0K}(CF_4)$.

[b]The calculated $AP_0(CF_3^+/CF_4)$ for $CF_4 \rightarrow CF_3^+ + F$ at W1 and CBS-APNO level using a weighted factor derived from the 0 K appearance energy of H-loss from $CH_2F_2^+$.

and quantum chemical calculations.[25,26] Table I summarizes the most experimental and recent calculated values of $AP_0(CF_3^+/CF_4)$ and obviously these data are in controversy. Therefore, to establish a more accurate $AP_0(CF_3^+/CF_4)$ in experiment and compare it with the high-level quantum chemical calculated data is a major aim of present work.

For dissociation of CF_4^+ ions in electronically excited states, an apparent electronic state-selectivity was found in previous investigations. By fitting TOF profile of CF_3^+ fragment ions, kinetic energy released distribution (KERD) in dissociation of CF_4^+ ions were evaluated.[5,18–21] Briefly, a nearly monoenergetic kinetic energy was released in dissociation of both X^2T_1 and A^2T_2 states, on the contrary fragmentation of CF_4^+ ions in B^2E state showed a wide distribution of released kinetic energy.[18] Furthermore, an induced radiative emission by electron impact was observed and surmised from $CF_4^+(B^2E)$ ion in the van Sprang and Brongersma's experiment.[28] However Maier *et al.* did not detect the expected visible fluorescence of $B^2E \rightarrow X^2T_1$ transition in a wavelength range of 200–900 nm.[16] Thus a reasonable explanation is necessary to understand energy redistribution in dissociation of B^2E state. In addition, anisotropic angular distribution of CF_3^+ fragment ions dissociated from CF_4^+ ions at fixed excitation energy less than 40 eV was observed recently with the method of ion imaging.[14] However, due to the lack of ionic state-selectivity, the measured CF_3^+ fragments were produced from dissociation of all energy-allowed electronic states of CF_4^+ and thus the anisotropic distribution should be a weighted mean of all involved ionic states. Using VIPCO technique, an anisotropic angular distribution of electrons were also analyzed for photoionization processes to form X^2T_1 and A^2T_2 ionic states.[15]

To understand dissociation of CF_4^+ ions in specific ionic state, a few quantum chemistry and dynamics calculations were performed.[29–32] Briefly, both X^2T_1 and A^2T_2 states are repulsive along the C-F coordinate and able to dissociate to $CF_3^+(X^1A_1)$ and $F(^2P)$ fragments, while the B^2E state is typical bound. These results are generally consistent with the previous experimental conclusions. Moreover, Beärda and Mulder suggested that there is a stable complex of $CF_3^+ \ldots F$ along the C-F coordinate of X^2T_1 state and hence $CF_4^+(X^2T_1)$ ions may survive a few vibrations prior to dissociation.[29] However, the lifetime of complex was found extremely short in a direct *ab initio* trajectory calculation.[31]

As an upgraded experimental approach, threshold photoelectron-photoion coincidence (TPEPICO) velocity imaging is powerful to analyze dissociation of energy-selected ions.[33] Compared with the method of fitting TOF profiles, more exact KERD and angular distribution of fragments dissociated from internal energy selected ions can be acquired directly from velocity map images,[34,35] and more details of dissociation dynamics are revealed, e.g., vibrational distribution of fragment ions.[36–39] In the present work, an experimental reinvestigation on dissociative photoionization of CF_4 in the excitation energy range of 15.40–19.60 eV is performed using TPEPICO velocity imaging. For CF_4^+ ions in X^2T_1, A^2T_2, and B^2E states, KERD and angular distributions of CF_3^+ fragment ions are measured, respectively. An adiabatic appearance potential $AP_0(CF_3^+/CF_4)$ has also been directly obtained in experiment and compared with the recent calculations. More importantly, dissociation mechanisms of specific ionic states of CF_4^+ are proposed in details with the aid of potential energy curves.

II. EXPERIMENTS

Present experiments were performed at the U14-A beamline of National Synchrotron Radiation Laboratory (Hefei, China). The configurations of the beamline and TPEPICO velocity imaging spectrometer have been introduced in details previously,[33] and thus only a brief description is presented here. Synchrotron radiation (SR) from an undulator was dispersed with a 6 m spherical-grating monochromator, in which a 370 grooves mm^{-1} grating was used to cover a photon energy range of 7.5–22.5 eV. A typical photon bandwidth is 6 meV in this energy range.[40] A gas filter filled with noble gas was used to reduce higher-order harmonic radiation of beamline.

A home-made 30-μm-diameter nozzle was utilized to generate continuous supersonic molecular beam (MB), which interacted with SR at right angle in photoionization chamber. Using a same dc extraction electric field, photoelectrons and photoions produced from DPI process were collected in opposite directions. A specially designed repelling electric field was used to magnify and map velocity image of electrons, and thus the contamination of energetic electrons was almost completely suppressed in TPES and TPEPICO measurement.[33] The typical photoelectron energy resolution is ∼9 meV. Photoions were projected onto multichannel plates (MCP, 40 mm

diameter) backed by a phosphor screen (Burle Industries, P20). A thermoelectric-cooling charge couple device camera (Andor, DU934N-BV) was used to record ion image on the screen. Once a threshold photoelectron was collected in experiment, a pulsed high voltage (DEI, PVM-4210) was applied at MCPs to act as mass gate, whose time origin and width were decided by TOF of target ion. In the following experiments, a typical 80 ns duration was used to record images of CF_3^+ fragment ions whose jitter was less than 2 ns. Thus the TPEPICO velocity image of fragment ions dissociated from specific internal energy selected parent ions could be recorded.

Commercial CF_4/Ne (1:9) mixture gas (Nanjing specialty gases) with a stagnation pressure of 2.0 atm was injected into the spectrometer. After collimated by a 0.5-mm-diameter skimmer, MB was intersected with SR at 10 cm downstream from the nozzle. The typical backing pressure in the photoionization chamber was better than 1×10^{-4} Pa with the MB on. The absolute photon energy of SR was carefully calibrated using the well-known ionization energies of noble gases, and a silicon photodiode (International Radiation Detectors Inc., SXUV-100) was used to record photon flux.

III. RESULTS AND DISCUSSION

A. Threshold photoelectron spectrum of CF_4

Threshold photoelectron spectrum of CF_4 with a step size of 12 meV in an excitation energy range of 15.40–19.60 eV has been measured, normalized to the photon flux, and presented in Fig. 1. Three observed bands are assigned to the lowest-lying three electronic states of CF_4^+ ions, X^2T_1, A^2T_2, and B^2E, respectively. The resonant energies and relative intensities of the bands are in good agreement with the previous results.[4,5] X^2T_1 and A^2T_2 bands are broadened and structureless in the spectrum. For B^2E band, a few weak peaks superimposed over a broadened background in the previous high-resolution TPES[4,5] are indistinct in Fig. 1. Four resonant energies are chosen and noted with stars in Fig. 1, in which two excitation energies within the X^2T_1 band, 15.98 eV and 16.38 eV, are specially selected in order to discuss its dissociation mechanism.

B. TPEPICO TOF mass spectra

TPEPICO TOF mass spectra of CF_4 are measured at photon energies of 15.98, 16.38, 17.54, and 18.48 eV, respectively, and presented in Fig. 2. None CF_4^+ parent ions is found, and only one TOF peak located at 17.2 μs is observed, which attributes to CF_3^+ fragment ions. Thus CF_4^+ ions in all the X^2T_1, A^2T_2, and B^2E states fully dissociate to produce CF_3^+ fragment ions, which agrees well with the previous measurements[5,18–20]. Furthermore, the second dissociation limit of $CF_3^+(A^1E) + F(^2P)$ is calculated at MP4(FC)/6-311+G(2df,p)//B3LYP/6-611G* level and 138 kcal $\cdot$ mol^{-1} (5.98 eV) higher in energy than that of the lowest $CF_3^+(X^1A_1) + F(^2P)$ channel. Since it is beyond the present excitation energy, only the lowest $CF_3^+(X^1A_1) + F(^2P)$ channel is taken into account in the following discussion.

With an extraction electric field of 14 V $\cdot$ cm^{-1}, the width of TOF profile for ions without kinetic energy released was only about 15 ns (full width at half maximum, FWHM).[33] Due to the kinetic energy release in dissociation of CF_4^+, the TOF widths of CF_3^+ fragment ions in Fig. 2 are obviously broadened to 690, 706, and 760 ns (FWHM) at 15.98, 16.38, and 17.54 eV, respectively. Interestingly, that at 18.48 eV of B^2E state is only 693 ns although the photon energy far exceeds both X^2T_1 and A^2T_2 ionic states, indicating that dissociative mechanism of $CF_4^+(B^2E)$ ions should be different from that of the X^2T_1 and A^2T_2 states. In addition, the TOF profiles of CF_3^+ are obviously changed with the photon energy. A near rectangular contour in Figs. 2(a)–2(c) is found for both X^2T_1 and A^2T_2 states, while it shows a triangular shape for CF_3^+ dissociated from $CF_4^+(B^2E)$ ions at 18.48 eV. Therefore, kinetic energy distribution of CF_3^+ fragment ions in dissociation of X^2T_1, A^2T_2, and B^2E states are expected to be different.

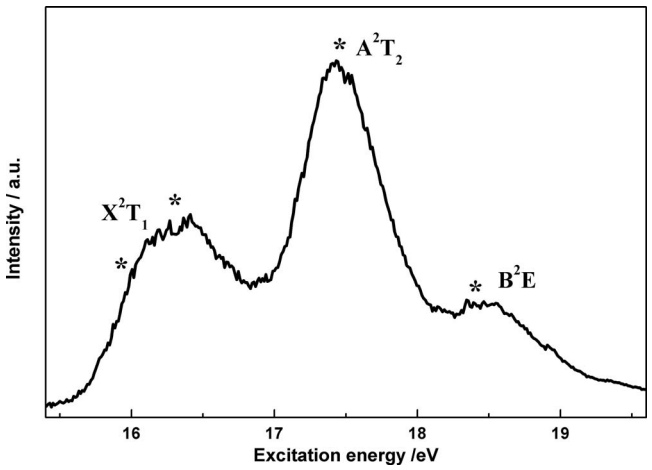

FIG. 1. Threshold photoelectron spectrum of CF_4 in the excitation energy range of 15.40–19.60 eV.

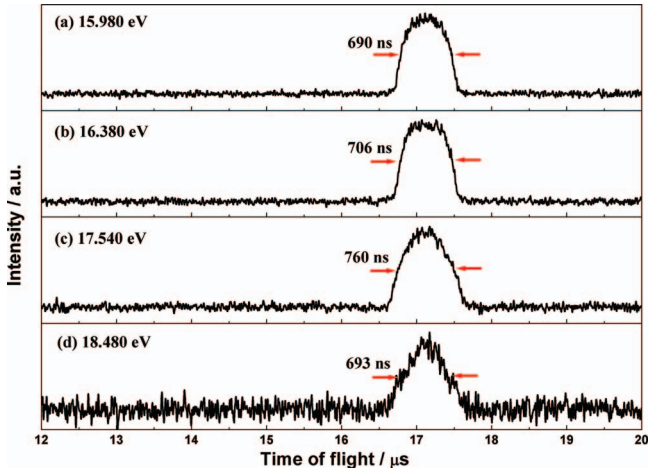

FIG. 2. Threshold photoelectron-photoion coincidence time-of-flight mass spectra for dissociative photoionization of CF_4 at photon energy of (a) 15.98 eV, (b) 16.38 eV, (c) 17.54 eV, and (d) 18.48 eV.

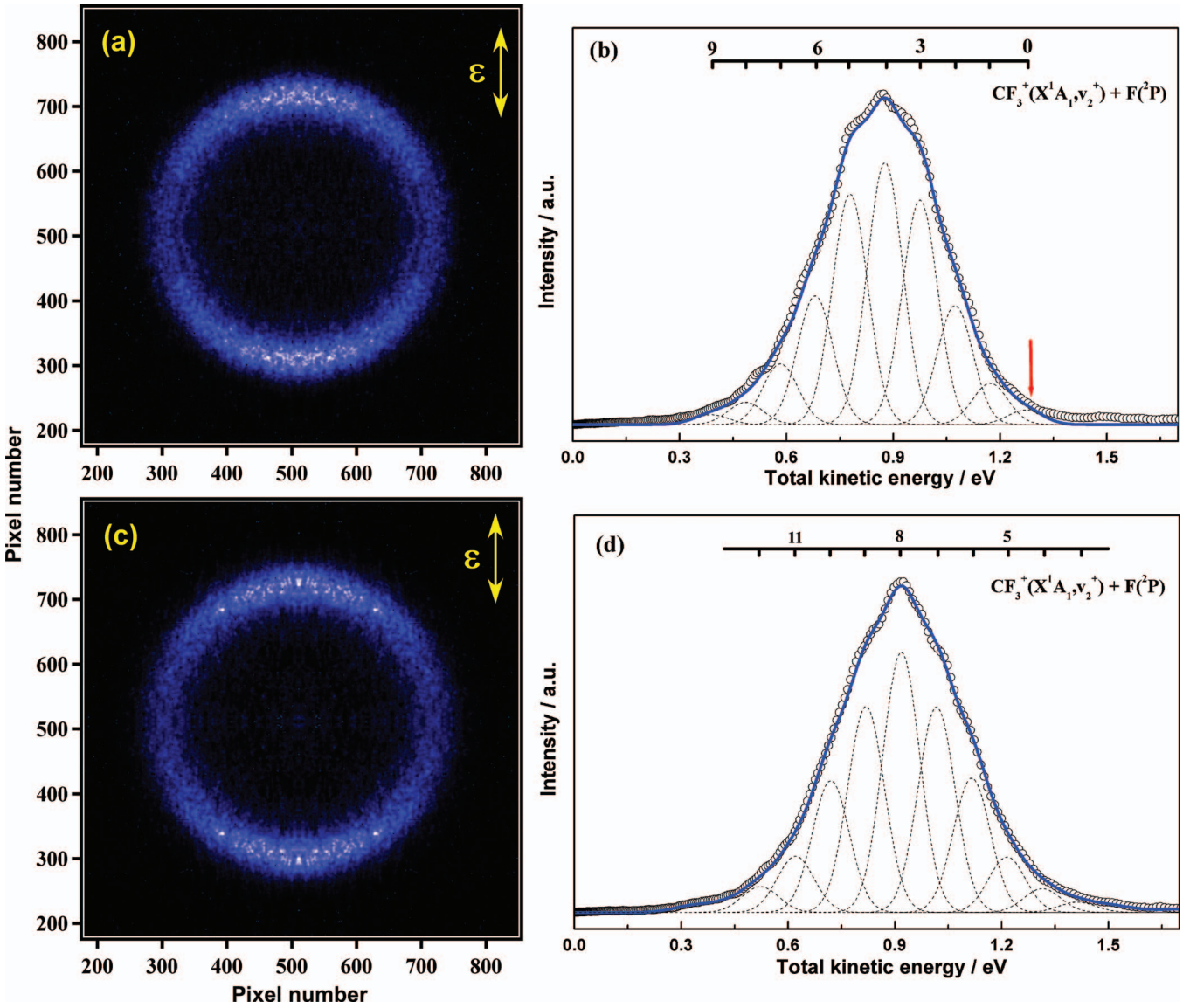

FIG. 3. Three-dimensional threshold photoelectron-photoion coincidence time-sliced velocity images of CF_3^+ fragments and the corresponding total kinetic energies released distributions in dissociation of $CF_4^+(X^2T_1)$ ions. (a) and (b) at 15.98 eV; (c) and (d) at 16.38 eV.

C. TPEPICO velocity images of CF_3^+ dissociated from $CF_4^+(X^2T_1)$ ion

As shown in Table I, the previous measured values of $AP_0(CF_3^+/CF_4)$ were inconsistent. Especially, the $AP_0(CF_3^+/CF_4)$ value obtained by Chim *et al.*[21] is far different from the other data,[18–20] although all of them were derived from photoelectron-photoion coincidence measurements. Fortunately, kinetic energy resolution of the present measurement is better than 3% of ΔE/E after a careful calibration of ion images using the well-known KERD in dissociation of $O_2^+(B^2\Sigma_g^-)$ ions,[33] and hence more dynamic details in dissociation of $CF_4^+(X^2T_1)$ ions can be revealed.

Figures 3(a) and 3(c) show the 3D TPEPICO time-sliced velocity images of CF_3^+ dissociated from the $CF_4^+(X^2T_1)$ ions at 15.98 eV and 16.38 eV, respectively. The polarization vector ϵ of photon is along vertical direction in the image. There is only one rough ring in both images, indicating that only a nearly monoenergetic distribution is released in dissociation. It is consistent with the previous experiments.[18–20] In addition, a parallel anisotropic distribution can be observed in the images, and thus dissociation of $CF_4^+(X^2T_1)$ ions should be rapid. By accumulating intensity of the image over angles, speed distribution of CF_3^+ fragment ions is acquired directly. From conservation of linear momentum, total KERD in dissociation of $CF_4^+(X^2T_1)$ ions at 15.98 and 16.38 eV can be subsequently obtained and shown in Figs. 3(b) and 3(d). Obviously, the diameter of ring in the images of Figs. 3(a) and 3(c) just slightly increases with excitation energy, and the maximal total kinetic energy of fragments only increases a little bit from 1.28 eV (at 15.98 eV) to 1.40 eV (at 16.38 eV). That means, more fraction of available energy in dissociation has been distributed to internal energy of fragments with

TABLE II. Mean total kinetic energy released $\langle E_T \rangle$ and anisotropic parameters β in dissociation of CF_4^+ ions in three low-lying electronic states.

hv (eV)	E_{avail} (eV)	$\langle E_T \rangle$ (eV)	f_T Expt.	f_T Theor.	β Previous[a]	β Present
15.98	1.27	0.85	0.67		...	0.64 ± 0.09
16.38	1.67	0.90	0.54	0.49[b], 0.65[c]	0.65 (16.5 eV)	0.72 ± 0.07
17.54	2.83	1.20	0.42		0.60 (17.5 eV)	0.95 ± 0.08
18.48	3.77	1.09	0.29		0.45 (18.5 eV)	0.51 ± 0.09

[a]From Ref. 14, where the corresponding excitation energies are shown in parentheses.
[b]f_T is calculated using the classical "impulsive model."
[c]f_T for dissociation of CF_4^+ in X^2T_1 state is derived from the direct *ab initio* dynamic calculation at the HF/6-311G(d,p) level in Ref. 31.

excitation energy increasing, which is in agreement with the recent Bodi *et al.*'s experimental conclusion.[41] A unique explanation of the phenomenon is existence of a shallow well on F-loss potential energy surface of X^2T_1 state. Thus the Chim *et al.*'s assumption[21] that the fractional KE released is independent of ionization energy is unreasonable.

Generally, the maximal total kinetic energy of fragments can give an upper limit of adiabatic appearance potential $AP_0(CF_3^+/CF_4)$. As indicated in Fig. 3(b), the upper limit should be around 14.7 eV. In the Franck-Condon region, $CF_4^+(X^2T_1)$ ions dissociate fast along the C-F bond rupture, and thus the umbrella vibration ($v_2^+ = 798.1$ cm^{-1})[42,43] of CF_3^+ is expected to be dominantly excited. Taking into account the total KERD and the upper limit of $AP_0(CF_3^+/CF_4)$, the maximal v_2^+ quantum number of $CF_3^+(X^1A_1)$ should be less than 10 at 15.98 eV. Therefore, the possible vibrational state population of CF_3^+ can be assigned and shown in Fig. 3(b) as well. In Fig. 3(b), the $v_2^+ = 3$–5 population can be clearly identified, while the other vibrational state populations are blurry in a certain extent due to overlap. Therefore, a typical occurrence of vibrational population reversion is found for CF_3^+ fragment at 15.98 eV, and the corresponding mean vibrational energy $\langle E_v \rangle$ is calculated to be 0.43 eV. The most populated vibrational state is located at $v_2^+ = 4$. Taking the total kinetic energy (1.27 eV) at $v_2^+ = 0$ level as shown with an arrow in Fig. 3(b), the value of $AP_0(CF_3^+/CF_4)$ is determined to be 15.98 – 1.27 = 14.71 eV. According to the kinetic energy resolution is lower than 4 meV (1.27 × 3% = 3.8 meV) and the photoelectron energy resolution is ~9 meV, the uncertainty of $AP_0(CF_3^+/CF_4)$ can be estimated as less than 20 meV. The present $AP_0(CF_3^+/CF_4)$ is very consistent with the previous experimental data in Table I[18–20] and exactly matches the value of quantum chemical calculations.[26] In addition, both KERDs in Figs. 3(b) and 3(d) have the similar contours without clear resolvable structures. The most populated vibrational state of CF_3^+ is changed from $v_2^+ = 4$ at 15.98 eV to $v_2^+ = 8$ at 16.38 eV.

Angular distribution of fragment ions can be derived from the integration of images over a proper range of speed at each angle. Consequently, anisotropic parameter β can be obtained by fitting the angular distribution. At 15.98 and 16.38 eV, both β values for CF_3^+ fragments are about 0.7 as shown in Table II, which is close to the previous data.[14] Thus dissociation of $CF_4^+(X^2T_1)$ ions shows a parallel tendency along the polarization vector.

D. TPEPICO velocity image of CF_3^+ dissociated from $CF_4^+(A^2T_2)$ ion

Because both outer $1t_1$ and $4t_2$ molecular orbitals of CF_4 molecule are consisted of the F lone-pair electron orbitals, characteristics of CF_4^+ in X^2T_1 and A^2T_2 states are similar. At 17.54 eV, CF_4^+ ions in the A^2T_2 state are produced and subsequently dissociate to CF_3^+ and F fragments. The recorded 3D TPEPICO time-sliced velocity image of CF_3^+ fragments dissociated from $CF_4^+(A^2T_2)$ ions is presented in Fig. 4(a). Only the lowest dissociation limit of $CF_3^+(X^1A_1) + F(^2P)$ can be opened at the excitation energy, and an unique rough ring is found in the image. The present image is very similar to the images of Figs. 3(a) and 3(c) indeed, except for its larger diameter.

From the image of Fig. 4(a), the total KERD in dissociation of $CF_4^+(A^2T_2)$ ions at 17.54 eV can be obtained and presented in Fig. 4(b). The maximal total kinetic energy of fragments increases to ~1.9 eV. Through fitting angular distributions of CF_3^+ as shown in Fig. 4(c), the corresponding anisotropic parameter β is determined to be 0.95. Therefore, dissociation of CF_4^+ ions in A^2T_2 state is parallel as well, and moreover the A^2T_2 ionic state has much shorter lifetime than X^2T_1 state. Due to the lack of ionic state-selectivity, Hikosaka

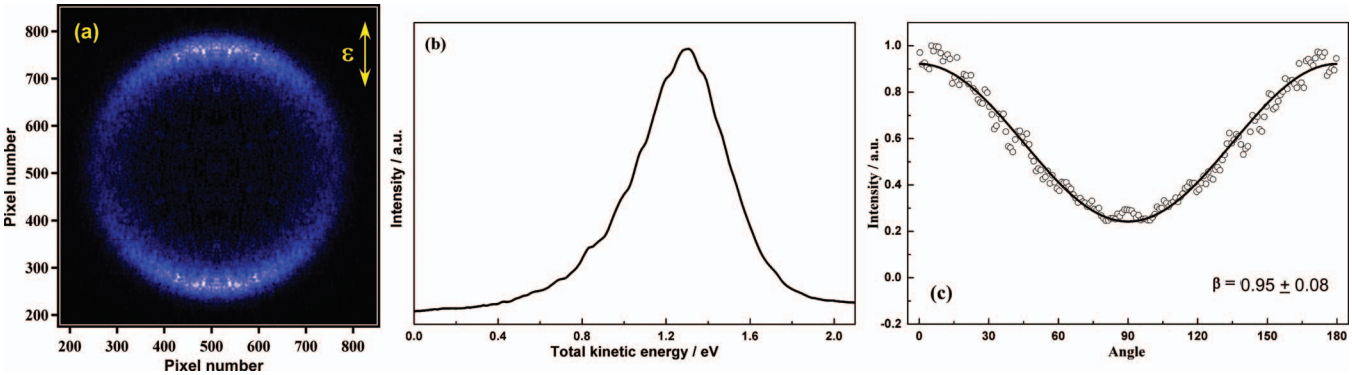

FIG. 4. 3D TPEPICO time-sliced velocity images (a) of CF_3^+ fragment ions, the corresponding total KERD (b) and angular distributions (c) in dissociation of $CF_4^+(A^2T_2)$ ions at 17.54 eV.

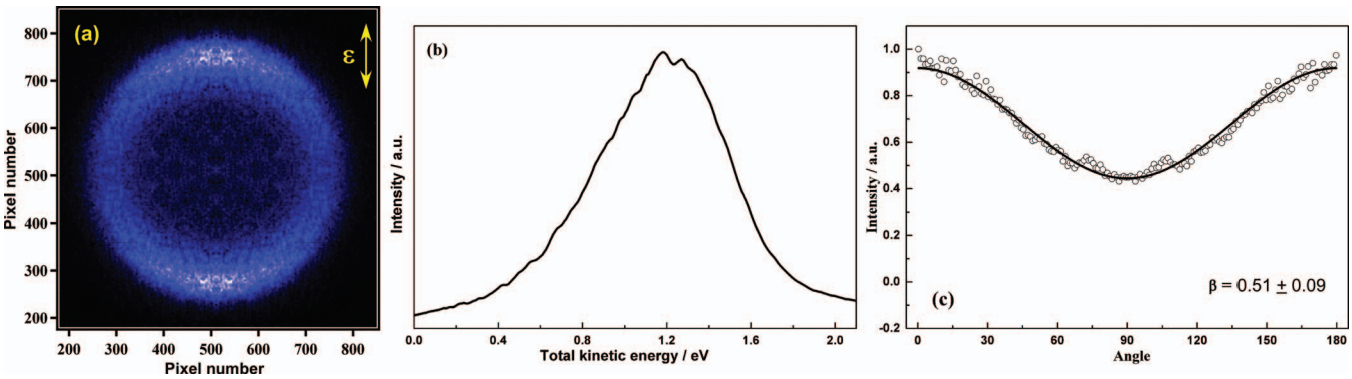

FIG. 5. 3D TPEPICO time-sliced velocity images (a) of CF_3^+ fragment ions, the corresponding total KERD (b) and angular distributions (c) in dissociation of $CF_4^+(B^2E)$ ions at 18.48 eV.

and Shigemasa[14] obtained a lower value of β (~0.6) than ours, and it was closer to it in dissociation of X^2T_1 state.

E. TPEPICO velocity image of CF_3^+ dissociated from $CF_4^+(B^2E)$ ion

Figure 5(a) shows the 3D TPEPICO time-sliced velocity image of CF_3^+ fragments dissociated from $CF_4^+(B^2E)$ ions at 18.48 eV. There is still only one rough ring observed whose width looks much wider than those from both X^2T_1 and A^2T_2 states, and hence the whole image becomes more diffusive. To our surprise, the maximal total kinetic energy of fragments for A^2T_2 and B^2E states are very close and even the most favorable kinetic energy released from B^2E state is slightly lower than that of A^2T_2 state as shown in total KERD curves, although the excess energy in dissociation of B^2E state is much larger than that of A^2T_2 state. Moreover, the anisotropic parameter β is decreased from 0.95 in A^2T_2 state to 0.51 in B^2E state, indicating that the lifetime of B^2E state is longer than those of the lower electronic states, X^2T_1 and A^2T_2.

F. Dissociation mechanism of CF_4^+ in the ground electronic state

Taking the adiabatic appearance potential $AP_0(CF_3^+/CF_4) = 14.71$ eV, the kinetic and internal energy distributions of CF_3^+ fragment ions dissociated from CF_4^+ ions can be derived from the images in Figs. 3–5. The mean total released kinetic energies $\langle E_T \rangle$ in DPI process at 15.98, 16.38, 17.54, and 18.48 eV, respectively, are calculated and summarized in Table II. The ratios of kinetic energy with available energy, f_T, can be calculated as 0.67 (15.98 eV), 0.54 (16.38 eV), 0.42 (17.54 eV), and 0.29 (18.48 eV).

If CF_4^+ ions dissociate fast along the C-F bond rupture with C_{3V} geometry, the dissociating time will not enough for intramolecular vibrational redistribution (IVR). Thus the classical "impulsive model" is expected to describe dissociation mechanism,[20] in which the proportion of mean total kinetic energy $\langle E_T \rangle$ and available energy E_{avail} can be calculated using the following formula:

$$f_T = \frac{\langle E_T \rangle}{E_{avail}} = \frac{\mu_{C-F}}{\mu_{CF_3-F}} = 0.49, \quad (1)$$

where μ is reduced mass. In dissociation, the C_{3V} geometry of CF_3 group is initially kept while F atom and CF_3 recoil sharply and effectively separate in a short time. Then umbrella vibration energy of CF_3^+ can be distributed from its initial recoiled kinetic energy. As list in Table II, the experimental f_T for dissociation of X^2T_1 state at 15.98 and 16.38 eV are 0.67 and 0.54, respectively, which exactly match the direct *ab initio* dynamic calculations at the HF/6-311G(d,p) level[31] and well compared to the value predicted with the "impulsive model." Specially, the mean vibrational energy $\langle E_v \rangle$ of CF_3^+ fragment ions in DPI process at 15.98 eV is 0.43 eV and high-J rotational excitation of CF_3^+ is not evident. Therefore, the angle θ between the leaving F atom and the C_{3V} axis of CF_3^+ moiety at the moment of dissociation should be about zero, which is also consistent with the conclusion of direct *ab initio* dynamic calculation.[31]

In addition, it is very interesting that f_T for dissociation of X^2T_1 state is slightly decreased with excitation energy increasing as shown in Table II. It is in contrary to a fast dissociation predicted with the classical "impulsive model" along a very steep dissociating potential energy surface, in which the fraction of excess energy is independent on excitation energy. As shown in the schematic F-loss potential energy curves of CF_4^+ (Fig. 6), a shallow minimum ($CF_3^+ \ldots F$

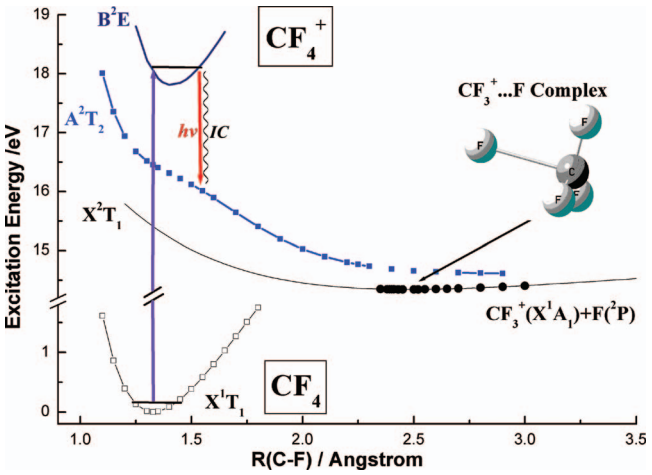

FIG. 6. Schematic F-loss potential energy curves of the low-lying electronic states of CF_4^+. The molecular structure of $CF_3^+ \ldots F$ complex is calculated at B3LYP/6-311G* level and shown as well.

complex) on potential energy surface of X^2T_1 ionic state along the C-F bond coordinate was suggested.[29–32] At B3LYP/6-311G* level, the dissociating C-F bond length of $CF_3^+ \ldots F$ complex is 2.50 Å and the corresponding bond angle θ(F-C-F) is 91.55°, which is far away from the Franck-Condon region. The energy of $CF_3^+ \ldots F$ complex is slightly lower (5.29 kcal · mol^{-1}) than that of final fragments, $CF_3^+(X^1A_1) + F(^2P)$. Although the density functional theory is unsuccessful for dispersive interaction in general, it looks still good for the ground state of CF_4^+ and the present results are in agreement with the high-level *ab initio* calculations.[31] For the $CF_3^+ \ldots F$ complex, the C-F bond length is found at 2.65 Å at MP4SDQ/6-311G(d, p) level, and its binding energy relative to the dissociation limit is 5.8 kcal mol^{-1} at the MP4SDQ/6-311G(d,p)//HF/6-311G(d, p) level.[31]

Therefore $CF_4^+(X^2T_1)$ ions will probably survive a few vibrational periods prior to complete dissociation. Especially in the Franck-Condon allowed lower energy region of X^2T_1 state, e.g., 15.98 eV or even less, the more notable binding interaction of the shallow well cause dissociation more adiabatically, in which the C-F bonds of CF_3^+ fragment are assumed to be infinitely rigid and hence much more excess energy is distributed in translation motion. Thus more fractional KE released is expected for the lower energy $CF_4^+(X^2T_1)$ ions, which is well consistent with the present experimental conclusions. On the other hand, we need to emphasize that the binding interaction of the complex is too weak to cause dissociating time obviously changed, as implied by the very close β values at 15.98 eV and 16.38 eV.

G. Dissociation mechanism of CF_4^+ in the low-lying electronically excited states

As indicated by both total KERD and angular distribution of fragments, dissociation mechanism of CF_4^+ ions in two low-lying electronically excited states, A^2T_2 and B^2E, are different. The A^2T_2 state is typical repulsive and adiabatically correlates to the lowest dissociation channel of $CF_3^+(X^1A_1) + F(^2P)$ (like X^2T_1 state). On the contrary, the B^2E ionic state is bound and adiabatically correlates with the excited state products, which are energetically inaccessible in the present energy range.

For the A^2T_2 ionic state, the potential energy surface is very steep in the Franck-Condon region and no complex is found along the C-F bond rupture, so that nuclear force drives CF_4^+ ion to dissociate impulsively. As shown in Table II, the fractional KE released is very close to the value predicted with the classical "impulsive model." Moreover, the measured anisotropic parameter β is 0.95 and larger than that of X^2T_1 state, indicating that dissociation of A^2T_2 state is faster indeed.

Compared with the cases of the X^2T_1 and A^2T_2 states, dissociation of the $CF_4^+(B^2E)$ ions is much complicated. As mentioned above, both the mean total released kinetic energy $\langle E_T \rangle$ and its fraction f_T of B^2E state at 18.48 eV are remarkably lower than those of A^2T_2 state at 17.54 eV (in Table II). Additionally, the maximal total kinetic energy of fragment dissociated from B^2E state is very similar to that from A^2T_2 state, although the excess energy is much larger. Therefore, partial excess energy of B^2E state must be released prior to dissociation.

As the B^2E ionic state is adiabatically bound, its dissociation must occur following internal conversion (IC) or radiative emission to a lower unbound electronic state. Taking into account the Franck-Condon factor, the more favorable unbound lower electronic state is the A^2T_2 state.[20] If $CF_4^+(B^2E)$ ion undergoes a primary IC process to A^2T_2 state, the high rovibrationally excited ion may be yielded prior to dissociation whose internal energy distribution is far from that through direct photoionization in Franck-Condon region. According to that the dissociating time along the steep A^2T_2 state is only within a few decade femtoseconds, the high rovibrationally excited CF_3^+ fragment can be produced and thus the total kinetic energy released from $CF_4^+(B^2E)$ is much lower than that along a direct dissociation process. Following a fast dissociation along the steep potential energy surface of A^2T_2, the invariable f_T value is expected (∼0.42 in Table II) for all vibrationally levels in Franck-Condon region. Therefore the most populated vibrational level of A^2T_2 state after decay of $CF_4^+(B^2E)$ ion can be estimated. At 18.48 eV (B^2E state), the measured $\langle E_T \rangle$ is 1.09 eV as shown in Table II, so that the excess energy prior to dissociation on the A^2T_2 potential energy surface will be 1.09/0.42 = 2.60 eV. From energy conservation, the mean released internal energy from B^2E can be calculated as 3.77 – 2.60 = 1.17 eV (∼1060 nm), where 3.77 eV is the excess energy at 18.48 eV above dissociation limit. Through the primary IC decay of B^2E state, the most populated vibrational level of the yielded A^2T_2 state prior to dissociation at 18.48 eV is located at an energy of 17.31 eV (18.48 – 1.17 eV), which is indeed lower than 17.54 eV (direct dissociation of A^2T_2 state as shown in Sec. III D). Thus the mean total released kinetic energy and f_T at 18.48 eV are certainly lower than those at 17.54 eV, which agrees well with the present measurement.

On the other hand, as van Sprang and Brongersma suggested,[28] B^2E state is long lived with a lifetime of several nanoseconds, and hence an emission decay of $CF_4^+(B^2E)$ ion seems also possible. $CF_4^+(A^2T_2)$ ion will be produced through the $B^2E \rightarrow A^2T_2$ fluorescence-emission at 18.48 eV. However, as indicated by the present β value (0.51) for dissociation of $CF_4^+(B^2E)$ ion, the lifetime of B^2E ionic state should be within picosecond range and much shorter than that suggested by van Sprang and Brongersma.[28] Therefore, emission-dissociation mechanism seems unreasonable and too slow to produce the remarkable anisotropic distribution of CF_3^+ fragment. It should be emphasized that the fluorescence observed by van Sprang and Brongersma[28] could be due to emission of neutral CF_3 or the IR decay of the hot CF_3^+ fragment ion.

Based on the discussion above, the dissociation pathway of electronically excited states, A^2T_2 and B^2E, can be summarized as follows:

$$CF_4^+(A^2T_2) \xrightarrow{\text{direct}} CF_3^+(X^1A_1) + F(^2P),$$

$$CF_4^+(B^2E) \xrightarrow{\text{IC}} CF_4^+(A^2T_2) \xrightarrow{\text{direct}} CF_3^+(X^1A_1) + F(^2P).$$

Just to be complete, there is no confessed indication to gainsay fluorescence from B^2E state up to now. In fact, the expected fluorescence wavelength (~1060 nm) of $B^2E \rightarrow A^2T_2$ is beyond the wavelength range of detector (200–900 nm) in Maier *et al.*'s experiment, which could cause them to unsuccessfully detect fluorescence.[16] To obtain a firm conclusion of decay mechanism of $CF_4^+(B^2E)$ ion, a new photoion fluorescence coincidence experiment is expected.

IV. CONCLUSION

Dissociative photoionization of CF_4 via the low-lying ionic electronic states, X^2T_1, A^2T_2, and B^2E, has been investigated using TPEPICO velocity imaging. In the excitation energy range of 15.40–19.60 eV, three electronic states are observed in TPES. Only CF_3^+ fragment ions are observed and its TOF profile is appreciably broadened in coincident mass spectra. Interestingly, both the TOF profile contour and width of CF_3^+ fragment ions dissociated from various electronic states are different.

3D TPEPICO time-sliced velocity images of CF_3^+ fragment ions dissociated from specific internal energy selected CF_4^+ ions are recorded at 15.98, 16.38, 17.54, and 18.48 eV, respectively. Both kinetic energy released distribution and angular distribution in dissociation of CF_4^+ ions have been obtained subsequently. For all the electronic states, X^2T_1, A^2T_2, and B^2E, the images of CF_3^+ fragments exhibit a parallel distribution along the polarization vector of photon.

For the X^2T_1 state, it is interesting that the maximal total kinetic energy of fragments only slightly increases from 1.28 eV (at 15.98 eV) to 1.40 eV (at 16.38 eV), indicating that more fractional available energy has been distributed to internal energy of fragments with excitation energy increasing. Thus a shallow minimum ($CF_3^+ \ldots F$ complex) far away from Franck-Condon region is proposed on the potential energy surface of X^2T_1, so that $CF_4^+(X^2T_1)$ ions should survive a few vibrational periods prior to complete dissociation. In addition, the vibrational state population of CF_3^+ is assigned by fitting the KERD curves. The most populated vibrational state of CF_3^+ via DPI at 15.98 eV is located at $v_2^+ = 4$, while it is increased to $v_2^+ = 8$ at 16.38 eV. Based on the obtained internal energy distribution of CF_3^+ fragments, an adiabatic appearance potential of $AP_0(CF_3^+/CF_4)$ at 14.71 ± 0.02 eV has been established and is very consistent with the recent calculated values.

For the electronically excited states, dissociation mechanisms of CF_4^+ ions have been proposed with the aid of F-loss potential energy curves. In A^2T_2 state, CF_4^+ ion dissociates impulsively along the steep potential energy surface to produce CF_3^+ and F fragments, and the corresponding dissociation mechanism is very close to the classical "impulsive model." However, dissociation of the bound B^2E state is more complicated. The maximal total kinetic energy of fragment dissociated from B^2E state is very similar to that from A^2T_2 state, and moreover both $\langle E_T \rangle$ and f_T are far lower than those for dissociation of $CF_4^+(A^2T_2)$ ions. Therefore, a two-step dissociation mechanism is suggested as follows: B^2E state initially converts to the lower A^2T_2 state via internal conversion, then CF_4^+ ion dissociates to CF_3^+ and F fragments along the steep potential energy surface of A^2T_2 state.

ACKNOWLEDGMENTS

The financial support is mainly provided by the National Natural Science Foundation of China (NSFC, Grant Nos. 10979042, 21027005, and 21073173) and National Key Basic Research Special Foundation (NKBRSF, Grant Nos. 2013CB834602 and 2010CB923300). X. Zhou also thanks the Fundamental Research Funds for the Central Universities (Grant No. WK2060030006) and USTC-NSRL Association funding (Grant No. KY2060030007). The China Postdoctoral Science Foundation (Grant No. 2012M511422) supports the work as well.

[1] C. R. Brundle, M. B. Robin, and H. Basch, J. Chem. Phys. **53**, 2196 (1970).
[2] D. R. Lloyd and P. J. Roberts, J. Electron. Spectrosc. Relat. Phenom. **7**, 325 (1975).
[3] D. M. P. Holland, A. W. Potts, A. B. Trofimov, J. Breidbach, J. Schirmer, R. Feifel, T. Richter, K. Godehusen, M. Martins, A. Tutay, M. Yalcinkaya, M. Al-Hada, S. Eriksson, and L. Karlsson, Chem. Phys. **308**, 43 (2005).
[4] A. J. Yencha, A. Hopkirk, A. Hiraya, G. Dujardin, A. Kvaran, L. Hellner, M. J. Besnard-Ramage, R. J. Donovan, J. G. Goode, R. R. J. Maier, G. C. King, and S. Spyrou, J. Electron Spectrosc. Relat. Phenom. **70**, 29 (1994).
[5] J. C. Creasey, H. M. Jones, D. M. Smith, R. P. Tuckett, P. A. Hatherly, K. Codling, and I. Powis, Chem. Phys. **174**, 441 (1993).
[6] T. A. Walter, C. Lifshitz, W. A. Chupka, and J. Berkowitz, J. Chem. Phys. **51**, 3531 (1969).
[7] J. C. Creasey, I. R. Lambert, R. P. Tuckett, K. Codling, L. J. Frasinski, P. A. Hatherly, M. Stankiewicz, and D. M. P. Holland, J. Chem. Phys. **93**, 3295 (1990).
[8] K. Stephan, H. Deutsch, and T. D. Märk, J. Chem. Phys. **83**, 5712 (1985).
[9] H. Deutsch, K. Leiter, and T. D. Märk, Int. J. Mass Spectrom. Ion Process. **67**, 191 (1985).
[10] Y. J. Kime, D. C. Driscoll, and P. A. Dowben, J. Chem. Soc. Faraday Trans. II **83**, 403 (1987).
[11] W. Z. Zhang, G. Cooper, T. Ibuki, and C. E. Brion, Chem. Phys. **137**, 391 (1989).
[12] E. R. Fisher and P. B. Armentrout, Int. J. Mass Spectrom. Ion Process. **101**, R1 (1990).
[13] M. Tichy, G. Javahery, N. D. Twiddy, and E. E. Ferguson, Int. J. Mass Spectrom. Ion Process. **79**, 231 (1987).
[14] Y. Hikosaka and E. Shigemasa, J. Electron. Spectrosc. Relat. Phenom. **152**, 29 (2006).
[15] T. Kinugawa, Y. Hikosaka, A. M. Hodgekins, and J. H. D. Eland, J. Mass Spectrom. **37**, 854 (2002).
[16] J. P. Maier and F. Thommen, Chem. Phys. Lett. **78**, 54 (1981).
[17] H. Biehl, K. J. Boyle, D. M. Smith, and R. P. Tuckett, Chem. Phys. **214**, 357 (1997).
[18] B. Brehm, R. Frey, A. Küstler, and J. H. D. Eland, Int. J. Mass Spectrom. Ion Phys. **13**, 251 (1974).
[19] I. G. Simm, C. J. Danby, J. H. D. Eland, and P. I. Mansell, J. Chem. Soc. Faraday Trans. II **72**, 426 (1976).
[20] I. Powis, Mol. Phys. **39**, 311 (1980).
[21] R. Y. L. Chim, R. A. Kennedy, R. P. Tuckett, W. D. Zhou, G. K. Jarvis, C. A. Mayhew, D. J. Collins, and P. A. Hatherly, Surf. Rev. Lett. **9**, 129 (2002).
[22] G. A. Garcia, H. Soldi-Lose, and L. Nahon, Rev. Sci. Instrum. **80**, 023102 (2009).
[23] G. Hagenow, W. Denzer, B. Brutschy, and H. Baumgärtel, J. Phys. Chem. **92**, 6487 (1988).
[24] R. L. Asher and B. Ruscic, J. Chem. Phys. **106**, 210 (1997).
[25] J. Csontos, Z. Rolik, S. Das, and M. Kállay, J. Phys. Chem. A **114**, 13093 (2010).
[26] A. Bodi, A. Kvaran, and B. Sztáray, J. Phys. Chem. A **115**, 13443 (2011).
[27] H. Dossmann, G. A. Garcia, L. Nahon, B. K. C. de Miranda, and C. Alcaraz, J. Chem. Phys. **136**, 204304 (2012).
[28] H. A. Van Sprang, H. H. Brongersma, and F. J. De Heer, Chem. Phys. **35**, 51 (1978).

[29]R. A. Beärda and J. J. C. Mulder, Chem. Phys. **128**, 479 (1988).
[30]R. A. Beärda, H. R. R. Wiersinga, J. F. M. Aarts, and J. J. C. Mulder, Chem. Phys. **137**, 157 (1989).
[31]H. Tachikawa, J. Phys. B **33**, 2367 (2000).
[32]J. M. G. de la Vega and E. San Fabián, Chem. Phys. **151**, 335 (1991).
[33]X. F. Tang, X. G. Zhou, M. L. Niu, S. L. Liu, J. D. Sun, X. B. Shan, F. Y. Liu, and L. S. Sheng, Rev. Sci. Instrum. **80**, 113101 (2009).
[34]H. Wang, X. G. Zhou, S. L. Liu, B. Jiang, D. X. Dai, and X. M. Yang, J. Chem. Phys. **132**, 244309 (2010).
[35]H. F. Xu, Y. Guo, S. L. Liu, X. X. Ma, D. X. Dai, and G. H. Sha, J. Chem. Phys. **117**, 5722 (2002).
[36]X. F. Tang, X. G. Zhou, M. L. Niu, S. L. Liu, and L. S. Sheng, J. Phys. Chem. A **115**, 6339 (2011).
[37]X. F. Tang, M. L. Niu, X. G. Zhou, S. L. Liu, F. Y. Liu, X. B. Shan, and L. S. Sheng, J. Chem. Phys. **134**, 054312 (2011).
[38]X. F. Tang, X. G. Zhou, M. M. Wu, S. L. Liu, F. Y. Liu, X. B. Shan, and L. S. Sheng, J. Chem. Phys. **136**, 034304 (2012).
[39]X. F. Tang, X. G. Zhou, M. M. Wu, Y. Cai, S. L. Liu, and L. S. Sheng, J. Phys. Chem. A **116**, 9459 (2012).
[40]S. S. Wang, R. H. Kong, X. B. Shan, Y. W. Zhang, L. S. Sheng, Z. Y. Wang, L. Q. Hao, and S. K. Zhou, J. Synchrotron Radiat. **13**, 415 (2006).
[41]A. Bodi, P. Hemberger, T. Gerber, and B. Sztáray, Rev. Sci. Instrum. **83**, 083105 (2012).
[42]Y. Pak and R. C. Woods, J. Chem. Phys. **106**, 6424 (1997).
[43]M. E. Jacox, J. Phys. Chem. Ref. Data **27**, 115 (1998).